

Review

Advances on Exploration Indicators of Mineral VNIR-SWIR Spectroscopy and Chemistry: A Review

Yan Zhou ^{1,2,*}, Tiangang Wang ^{1,2} , Feipeng Fan ^{1,2} , Shizhong Chen ^{1,3}, Weimin Guo ^{1,2}, Guangfu Xing ^{1,2}, Jiandong Sun ^{1,2} and Fan Xiao ^{1,2}

¹ Nanjing Center, China Geological Survey, Nanjing 210016, China; wangtg1899@gmail.com (T.W.); fanfp1111@163.com (F.F.); cshizhong@mail.cgs.gov.cn (S.C.); mwguo@163.com (W.G.); njxgfu@163.com (G.X.); njsunjiandong@163.com (J.S.); xiao163fan@163.com (F.X.)

² Research Centre for Pacific Rim Strategic Mineral Resources, Nanjing 210016, China

³ Urumqi Comprehensive Survey Center of Natural Resources, China Geological Survey, Urumqi 830000, China

* Correspondence: zhouy@mail.cgs.gov.cn

Abstract: Establishing exploration vectors to infer the properties of ore-forming fluids, locate blind ore bodies with the aid of visible to near-infrared (VNIR) and short-wave infrared (SWIR) spectroscopy, and infer the chemistry of minerals, is a new research interest for economic geology. Common alterations and clay minerals, including sericite, chlorite, epidote, alunite, kaolinite, tourmaline, etc., are ideal objects for the study of exploration indicators due to their sensitivity to variations in the nature of hydrothermal fluid. The diagnostic spectral feature and chemistry vary spatially and systematically with physicochemical change. VNIR spectroscopy can characterize the REE-bearing clay minerals directly. Obtaining spectral or chemical parameters with the aid of VNIR-SWIR spectroscopy, electron probe micro-analyzer (EPMA) or laser ablation inductively coupled plasma mass spectrometry (LA-ICP-MS) can help to establish exploration vectors. This paper systematically summarizes recent advances in mineral exploration indicators (MEIs) of VNIR-SWIR spectroscopy and chemistry, and compares them in different regions or deposits. We found that some MEI spatial variation trends are random, even the same type of deposit can show an opposite trend. The controlling factors that limit the application of the established MEIs are vague. Conducting further research on petrology and mineralogy with the aids of observation under microscopy, X-ray diffraction (XRD), TESCAN Integrated Mineral Analyzer (TIMA), and EPMA are suggested to discover alteration mineral assemblage, alteration stages, and behaviors of “the pathfinder elements” related to mineralization. Based on the above research, the physicochemical properties of ore-forming fluids and their control over MEIs can be inferred. Refining the theoretical basis is critical to understanding and popularization of spectral and chemical MEIs.

Keywords: VNIR-SWIR and mineral chemistry; exploration indicators; controlling factors; advances; research directions



Citation: Zhou, Y.; Wang, T.; Fan, F.; Chen, S.; Guo, W.; Xing, G.; Sun, J.; Xiao, F. Advances on Exploration Indicators of Mineral VNIR-SWIR Spectroscopy and Chemistry: A Review. *Minerals* **2022**, *12*, 958. <https://doi.org/10.3390/min12080958>

Academic Editor: Mercedes Suárez

Received: 14 June 2022

Accepted: 25 July 2022

Published: 28 July 2022

Publisher's Note: MDPI stays neutral with regard to jurisdictional claims in published maps and institutional affiliations.



Copyright: © 2022 by the authors. Licensee MDPI, Basel, Switzerland. This article is an open access article distributed under the terms and conditions of the Creative Commons Attribution (CC BY) license (<https://creativecommons.org/licenses/by/4.0/>).

1. Introduction

Arising from the era of blind ore body exploration, exploration technology based on the characteristic parameters of minerals was born. Short-wave infrared (SWIR) spectroscopy with high resolution can detect characteristic spectral absorption by particle vibrations from sources such as hydroxyl (OH⁻), carbonate (CO₃²⁻), and possible water molecules (H₂O) in target minerals [1–4]. The visible to near-infrared (VNIR) region includes sharp absorption bands of REE-bearing minerals, which are mostly the result of 4f-4f intraconfigurational electron transitions [5–8]. The above spectral features will help confirm the mineral species and relative content effectively. The shift of the SWIR feature absorption peak also reflects the feature of ion substitution in the mineral lattice. Modern mineral LA-ICP-MS micro-region in situ analysis technology can obtain information on the variety of element content

in the tens of micron intervals of a single mineral [3,9–12]. Combining VNIR-SWIR and LA-ICP-MS can obtain spectral parameters and chemical parameters that vary systematically with the spatial change of physicochemical conditions. Mineral exploration indicators (MEIs) can be established after extracting those parameters comprehensively, which is an effective tool for predicting mineralization centers and locating blind ore bodies [10,12–16].

Alteration minerals, as the footprints of the hydrothermal mineralization process, are the focus of ore geology and exploration indicator research [12,17–24]. The properties of alteration minerals are more stable than bulk-rock, thereby allowing for the direct indication of the mineralization process. The alteration scale is generally much larger than the ore body. Effective alteration mineral exploration indicators can largely expand the scope of prospecting forecasting and help understand the metallogenic mechanisms and hydrothermal evolution processes precisely [16,25].

Since 2000, Australia, the United Kingdom, China, and other countries have begun to research exploration indicators with the aid of spectroscopy and mineral chemistry [2–4,12,25–27]. Recently, the research on “alteration mineral exploration identification” led by the National Mineral Research Center of the University of Tasmania in Australia has yielded some noteworthy achievements [12,16,28]. However, the mineralization is in an open system where the chemical variation of alteration minerals is controlled by multiple factors such as hydrothermal fluid conditions (temperature, pressure, oxygen fugacity, pH, etc.) and protolith properties, and the variation rules in different regions or deposits are not the same. So far, the main control factors for most of the systematic changes in mineral chemistry observed are still unclear. More research cases and multi-method combinations are needed to understand the MEIs, which is significant for refining the theoretical basis.

2. Research Advances and Problems of MEIs

The target minerals for MEI research mainly include sericite, chlorite, epidote, alunite, REE-bearing minerals, pyrite, quartz, tourmaline, and calcite. Specific research objects are often selected according to different mineralization types and alteration features. The target mineral must be widely available and be sensitive to changes in the physicochemical environment.

The common spectral MEIs include sericite Al-OH absorption peak (Pos2200) shift and illite crystallization (IC) [1,2,29–36], chlorite Fe-OH absorption peak (Pos2250) shift [1,4,33,37–40], alunite 1480 nm absorption peak (Pos1480) shift [3,41] and REE-bearing mineral absorption features at the bands of 640–870 nm [5–8,42]. The common chemical MEIs include contents of Ti, Sr, Mn, Pb, and their ratio values in chlorite [4,43–47], contents of Si, Al, Mn, Zn, and their ratio values in sericite [30,48], contents of As and Sb, and their ratio values in epidote [45,46,49] and contents of K, Na, La, Sr, Pb, and their ratio values in alunite [3,41]. Meanwhile, contents of Al and Ti in quartz, contents of Sn, Li, Ni, V, and Zn in tourmaline, and contents of Cl and F in biotite are also potential exploration indicators [50–53].

Illite crystallization (IC) is a terminology proposed by Kübler (1967) [54], which refers to the ratio of Pos2200 peak depth to near 1900 nm absorption (Pos1900) peak depth of sericite (Figure 1). IC value can be used to indicate the formation temperature of sericite. The higher the IC value, the less water content the mineral contains and the higher the formation temperature [2]. The shift of Pos2200 reflects the substitution of Si and Al in the tetrahedral and the substitution between Al, Mg, and Fe in the octahedral of the sericite lattice. Pos2200 value decreases with the increase of Al content in the lattice (Figure 2a). The shift of Pos2250 reflects the substitution of Al, Mg, and Fe in the octahedral of the chlorite lattice. Pos2250 value increases with the increase of Fe content in the lattice [55–57] (Figure 2b). The shift of Pos1480 reflects the substitution of K and Na in the alunite lattice. Pos1480 value increases with the increase of Na content in the lattice [3,58] (Figure 2c). The REE-bearing mineral absorption features reflect rare earth element anomalies and protolith variations. In addition, there are also extensive substitutions of interlayer ions and trace elements such as Ti, Sr, Mn, Pb, and Zn, and their substitution characteristics can be obtained by LA-ICP-MS and EPMA in situ micro-regions.

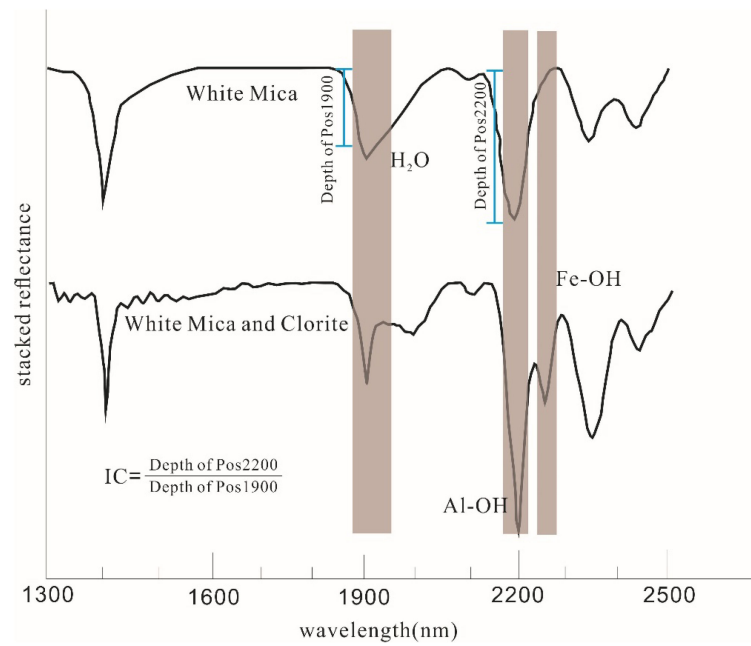


Figure 1. Typical SWIR absorption spectra (Hull quotient corrected) of white mica and a mixture of white mica and chlorite (modified from [1]), showing the absorption band position and depth of Al-OH, Mg-OH, and H₂O (hygroscopic water).

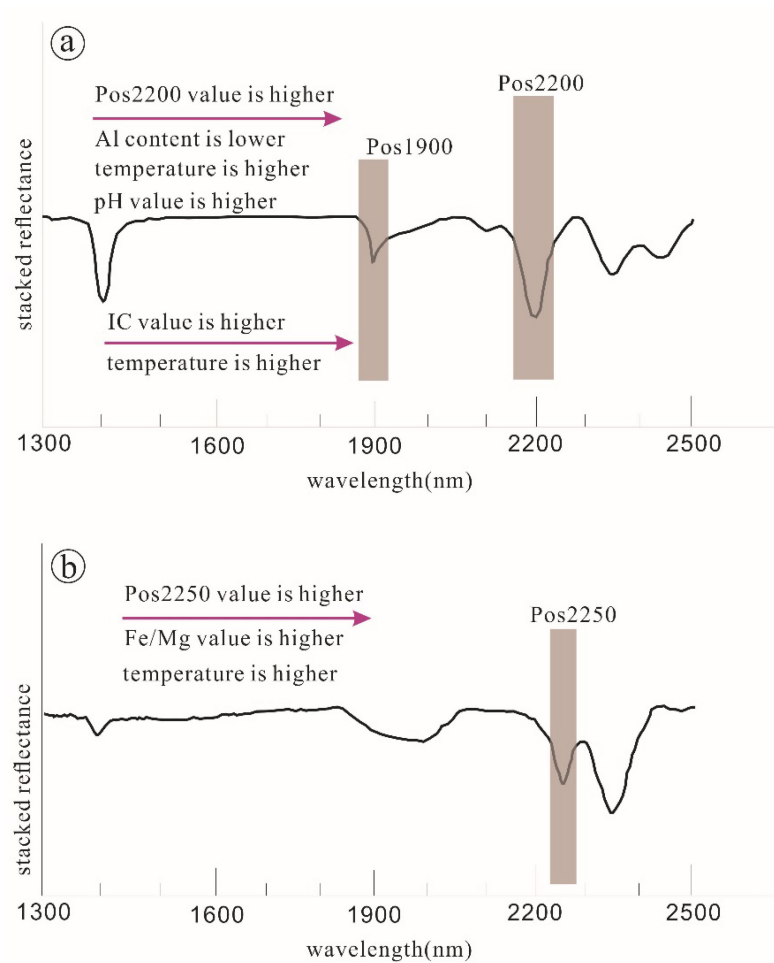


Figure 2. Cont.

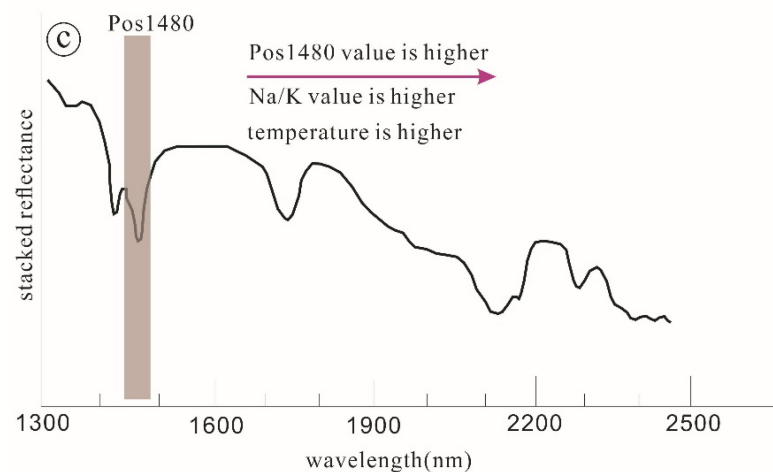


Figure 2. Schematic showing the correlation between the shift of diagnostic absorption peak, mineral chemistry, and controlling factors. (a)—correlation of the Pos2200 value, the Al content, temperature, the pH value, and the IC value of sericite; (b)—correlation of the Pos2250 value, the Fe/Mg value, and temperature of chlorite; (c)—correlation of the Pos1480 value, the Na/K value, and temperature of alunite.

2.1. Exploration Indicator of Sericite

Sericite is the most common indicative alteration mineral in magma-hydrothermal type deposits. Illite and fine-grained light-colored mica with hydrothermal origin are often collectively referred to as "sericite." Sericites are mainly developed in the sericitic phyllic zone of porphyry deposits, and are an important sign of the transition from the alkaline alteration stage to the acidic alteration stage. During the sericite alteration stage, the concentration of alkali metal ions, pH, and temperature of the ore-forming fluid are reduced, and the stability of the metallogenic element complex is greatly reduced, which results in the unloading of Cu, Au, Mo and their accompanying critical elements, As, Re, Se, and Te. For most ore bodies of low sulfidation (LS)—intermediate sulfidation (IS) epithermal deposits occurred in the illite–smectite zone. A large number of ion substitutions occurred in sericite during alteration, suggesting sericite is extremely sensitive to the changes in the hydrothermal environment. The subspecies—illite, muscovite, and phengite—formed in different physicochemical environments. Exploration indicators—Pos2200 and contents of Si, Al, Ti, Sr, Mn, Pb, and Zn—are usually applied in two major types of “porphyry” and “epithermal” mineralization systems. The combination of SWIR and chemistry vectors are proposed to indicate mineralization centers, indicate heat sources, locate ore bodies, and infer hydrothermal fluid properties and mineralization types.

According to the research on typical Cu-Au porphyry deposits of Yerington, Red Chris, Galore Creek, Butte, Christmas, and Highland Valley, Halley et al. (2015) [26] found Pos2200 value reduces regularly from the core of ore body upwards with a range of 2210–2200 nm, inferring that the composition of phengitic muscovite gradually decreased. From the host rock to the wall rock, an opposite change is presented [26] (Figure 3). The regular variation of Pos2200 value is controlled by Tschermak substitution [59]: $\text{Si}^{\text{iv}}(\text{Fe}, \text{Mg})^{\text{vi}} \leftrightarrow \text{Al}^{\text{iv}} \text{Al}^{\text{vi}}$ (iv and vi represent tetrahedral and octahedral coordination numbers, respectively). Generally, when the hydrothermal fluid migrated from deep to shallow, the fluid property evolved from a neutral condition to an acidic condition, and the pH value gradually decreased. Meanwhile, when the fluid migrated laterally to the wall rocks, the water/rock ratio decreased rapidly, and the pH value was buffered by the surrounding rock [26]. Yang et al. (2012) [2] used $\text{IC} \geq 1.6$ and $\text{Pos2200} \leq 2203$ nm as indicators to infer a higher fluid temperature and a mineralization potential in the northeast area of the Niancun porphyry Cu deposit, Tibet, China. Tian et al. (2018) [34] also found similar rules in the Gangjiang porphyry Cu-Mo deposit, Tibet, where a higher IC value (≥ 1.5) and lower pos2200 value (≤ 2205 nm) appeared near the ore bodies. Pos2200 value has a good

correlation with Cu-Au grade in the Chating porphyry Cu-Au deposit of Anhui province, China, which can help to interpret fluid evolution combined with the ore geology: there are no significant spatial changes in Pos2200 value and the Cu-Au grade is barren or low in depth, reflecting stable physicochemical conditions. After the fluid upflowed to the shallow level, the fluids migrated along several channels respectively. The pH of the fluid is relatively lower, the sericite is Al-rich, and the Pos2200 value is lower in the channel interior, where high-grade Cu-Au mineralization occurred. Relatively, the pH and Pos2200 values are higher in the channel exterior due to the buffer of surrounding rocks [36].

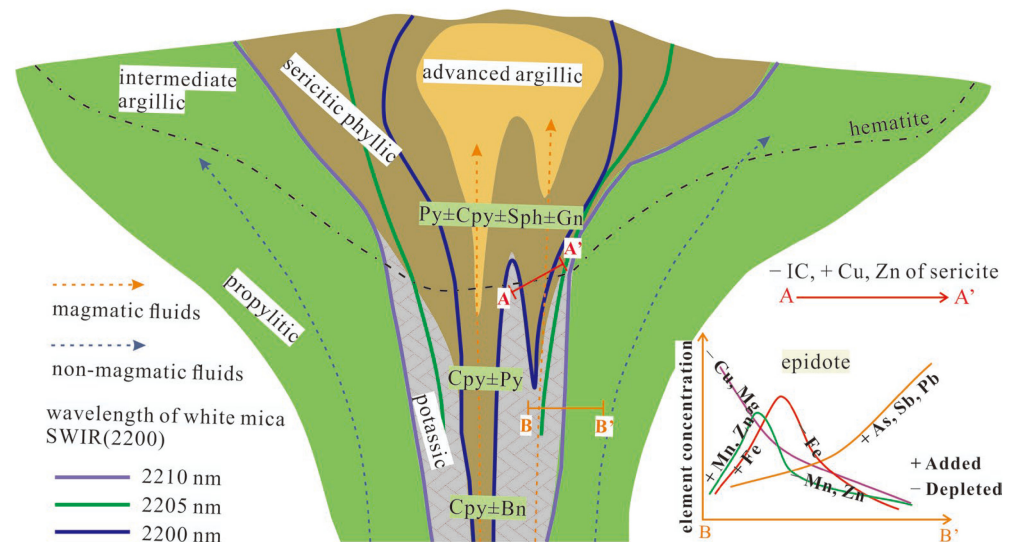


Figure 3. Vertical cross section of a typical porphyry Cu deposit showing the distribution of hydrothermal alteration, sulfide minerals, and generalized contours of the 2200 nm peak (modified from [26]). Also shown are generalized spatial variations in mineral chemistry of sericite and epidote. Cpy—chalcopyrite; Bn—bornite; Py—pyrite; Sph—sphalerite; Gn—galena.

In the porphyry Cu-Mo deposit of the Highland Valley region, Canada, the sericite with a lower Pos2200 value belongs to light-gray phengitic muscovite that coexists with bornite–chalcopyrite–molybdenite assemblage, suggesting a higher formation temperature and Na-rich composition. The sericite with a higher Pos2200 value is grey-green and mainly occurred in the phyllic zone. Cu and Zn contents and their ratio in sericite vary regularly with the distance from the porphyry center: the contents of Cu and Zn near the porphyry center are the lowest, possibly because the availability of H₂S leads to the precipitation of Cu-Fe sulfide minerals, reducing the Cu content in the fluid. The higher alteration temperature at the porphyry center tends to result in Zn being distributed around the periphery of the deposit [26,60] (Figure 3). This research supplies a useful vector for the exploration of porphyry Cu deposits. Additionally, the contents of Tl and Rb in sericite have a positive correlation but are not correlated to mineral paragenesis and spatial location, which may reflect that fluid composition and temperature are primary control factors for the behaviors of Tl and Rb, that are less affected by the surrounding rocks [48].

The SWIR and chemical features of the Laowangou Au deposit in the Qinling orogenic belt are very different from the magmatic-hydrothermal Au deposit, which is proposed to be evidence for the metamorphic genesis of the deposit. Pos2200 > 2210 nm and IC > 1.2 are available vectors for high-grade (>1 g/t) Au ore bodies [47]. Pos2200 of the Sunrise Dam and Kanowna Belle orogenic Au deposits in western Australia present regular variation, together with Au mineralization and key alteration minerals such as quartz, chlorite, carbonate, and sulfide. Sericite of the Kanowna Belle Au deposit is dominated by phengitic muscovite, and the fluid is alkalic, oxidized, and Si-rich. Sericite of the Sunrise Dam Au deposit is mainly composed of Na-rich muscovite and normal muscovite, and the fluid is acidic, reduced, and Na-rich with a higher Fe/(Fe + Mg) value. High-resolution SWIR

spectroscopy can measure Tschermak substitution effectively, which can be used as a useful vector tool for mapping alteration at Archean Au mineralization systems [30].

The above cases show two opposite Pos2200 trends: (1) the Pos2200 value decreases as the distance to the mineralization center decreases [1,2,57,61], and (2) the Pos2200 value increases as the distance to the mineralization center decreases [62–66]. Otherwise, there is no obvious correlation between Pos2200 and the distance to the mineralization center in some cases [67–69]. The main factors controlling the spatial variation of Pos2200 have not been identified, and the knowledge of the behaviors of trace elements such as Cu, Zn, Tl, and Rb of sericite is based only on the observation of limited data, lacking the evidence and interpretation from other studies such as petrology and mineralogy.

Most cases show the same change rule of IC: the IC value becomes larger near the mineralization center and smaller outwards. In the ideal environment where only sericite exists, accurate and reliable IC value calculation results can be obtained by using the relevant absorption parameters measured by SWIR spectroscopy, and the crystallinity degree and formation temperature of sericite can be finely characterized by the IC value. However, the actual alteration minerals are fine-grained and various, resulting in spectral curves mixed by various minerals. Pos1900 (caused by hygroscopic water) is jointly contributed by sericite, chlorite, and other hydrous minerals (Figure 1). The interference to Pos1900 must be eliminated before calculating the IC value, but it is difficult to perform in practice. At the same time, the concept of clay mineral crystallinity originated from low-grade metamorphic petrology. The higher the temperature, the weaker the IC value change, and the indication of the formation temperature will be limited, hence, the successful application of IC value is usually obtained by the epithermal systems.

2.2. Exploration Indicator of Chlorite

Chlorite, as a hydrous aluminosilicate mineral, is a kind of common alteration mineral in the intermediate to low temperature hydrothermal mineralization environment. Hydrothermal chlorite, dominant in the prophylic zone, is a critical sign for the exploration of porphyry deposits. Biotite, amphibole, and other mafic minerals are easily altered by chlorite. Chlorite alteration under different physicochemical conditions produces Mg-rich chlorite, Fe-rich chlorite, and general chlorite, indicating significant ion substitution between Mg and Fe in the chlorite lattice, accompanied by content variations of trace elements such as Ti, Sr, Mn, Pb, Zn, La, and Sr, spatially.

Chlorite can be used as an exploration indicator in porphyry type, skarn type, VMS type, and orogenic deposits. In the porphyry system, the changes of trace element content such as Ti and Sr can effectively approximate the porphyry or heat source that produces chlorite alteration. The contents of Cu, Pb, Sr, Ca, and Li can distinguish between hydrothermal and metamorphic chlorite. The shift of Pos2250 can be used to indicate ore bodies or mineralization centers in the skarn, VMS, and orogenic deposits.

Based on high-density sampling and systematic analysis, He et al. (2018) [43] found the contents of Ti, Ba, Co, K, Pb, Sr, Fe, and V/Ni values in chlorite are higher near the mineralization center of the Shaxi porphyry Cu-Au deposit in the Yangtze River metallogenic belt. The contents of Mn and Mg present an opposite trend [43]. Pacey et al. (2020) [70] found the concentrations of chalcophile elements (Cu, Pb, etc.) of chlorite can be used to distinguish between metamorphic and hydrothermal chlorite in the North Parkes porphyry mineralization system, Australia. The Mn and Zn contents of chlorite formed a peak halo at about 800 meters of the mineralization center (Figure 4). Combined with the ore geology, ore-forming fluid property, and the law of element migration, preliminary interpretations of the geochemical behaviors of relevant elements can be made [70].

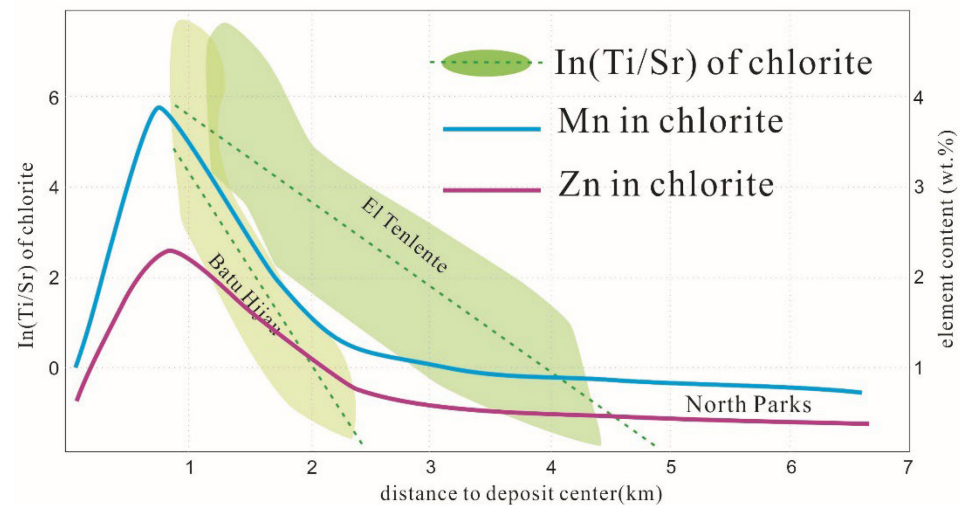


Figure 4. Schematic showing the natural log of the Ti/Sr ratio and the spatial variations of Mn and Zn contents in chlorite as functions of radial distance from the centers of El Teniente, Batu Hijau, and North Parks (modified from [9,45]).

The concentrations of Zn and Mn in chlorite also can identify metamorphic or hydrothermal chlorite at the El Teniente porphyry Cu mineralization system, Chile. Based on spatially systematic sampling and analysis of chlorite, the linear negative correlation between Ti/Sr value and distance from mineralization center is observed, suggesting chlorite Ti/Sr value is a powerful indicator for approaching the heat source [9,45,71] (Figure 4). Cooke et al. (2020) [72] conducted a blind test of chlorite Ti/Sr indicator to predict the mineralization center of the Resolution porphyry Cu-Mo deposit, Arizona, USA. Limited chlorite samples from drill holes are tested by LA-ICP-MS and an empirical formula for calculating the distance to the mineralization center is obtained based on Ti/Sr data and their spatial positions. The result showed that the gap between the inferred mineralization center and the factual mineralization center was less than 200 m [72]. Similar variation rules of Ti and V content and Ti/Sr value from mineralization center to periphery were documented in the Batu Hijau porphyry Cu-Au deposit, Indonesia, the North Parkes porphyry Cu-Au deposit, Australia and the Tuwu–Yandong porphyry Cu deposits, Xinjiang, China. However, the slopes of the formula in different deposits are not the same due to their geological features.

Chen et al. (2019) [4] suggested that $\text{Pos}_{2250} > 2249$ nm and $\text{Pos}_{2340} > 2333$ nm can be used as effective exploration indicators in the Tongshankou skarn–porphyry Cu-Mo-W deposit, Hubei province. Fe-rich chlorite is a useful exploration vector for the Tonglvshan skarn Fe-Cu-Au deposit in Southeast Hubei [4].

The factors that control Fe content in chlorite include temperature (Fe content is positively correlated with temperature), Fe content of the precursor minerals (e.g., biotite), and Fe content in hydrothermal fluids [9,57,69,73]. Even though the concentrations of some trace elements and Ti/Sr values in chlorite present obvious spatial regularity in typical porphyry systems, most deposits have undergone multi-stage alteration superposition and later reformation. Whether exploration indicators such as Pos_{2250} and Ti/Sr ratio are effective in those deposits needs further verification. At the same time, it is significant to understand the migration law of “the pathfinder elements” by combining the specific geological setting and mineralogy study.

2.3. Exploration Indicator of Epidote

Epidote, which is the altered product of plagioclase, hornblende, pyroxene, and the like, is common in porphyry systems. Epidote can also replace early-stage alteration minerals such as garnet and diopside in skarn deposits. Several element content variations of epidote can be used as proximitors to the blind porphyry or heat source. The contents

of As, Sb, and Pb rise with distance from the porphyry, while the contents of Cu and Mg decrease. Contents of As and Sb in epidote appeared abnormal in the range of 4 to 5 km away from the porphyry body, but bulk-rock geochemistry does not detect any anomaly. In addition, the content of As and Mn can help with judging the deposit scale and type. Compared with metamorphic epidote, the contents of Ca and Mn associated with the propylitic zone are higher [70].

Wilkinson et al. (2015, 2020) [9,45] found the Protolith composition had little effect on the epidote chemistry of the El Teniente porphyry Cu-Mo deposit, Chile. The Fe content shows a clear spatial variation law, gradually rising from the mineralization center to the periphery, reaching a maximum at about 1 km from the mineralization center, and then gradually decreasing [9,45] (Figure 3). Except for Ba, Pb, Sr, and Zr, the contents of other elements in epidote that occurred in different rocks are similar. Further interpretation is needed to understand those geochemical behaviors. The Mn and Pb contents in epidote, together with the Mn and Zn contents in chlorite, formed an Mn-Pb-Zn peak halo at about 800 m outside the mineralization center of the North Parkes porphyry system, Australia [70].

2.4. Exploration Indicator of Alunite

Alunite is a kind of indicative alteration mineral in epithermal deposits, whose formation is due to strong acidic leaching. Alunite, together with pyrophyllite and quartz, constitutes the lithocap, which is defined by a large range of native siliconization, advanced argillic, and intermediate argillic zones. As an important prospecting indicator, lithocap often develops HS-IS epithermal deposits and is closely associated with porphyry Cu-Au deposits and secondary Cu deposits [16,74]. Na/(Na + K) value and Pos1480 value of alunite have a positive correlation, with higher Pos1480 value corresponding to higher Na content [58]. Higher Na content in alunite implies higher formation temperature, which is experimentally proven [75] (Figure 2c).

Chang et al. (2011) [3] documented the variation of Pos1480 and Na/(Na + K) values in the Lepanto HS epithermal Cu-Au deposit, Philippines: K-rich alunite results in lower Pos1480 value, and Na-rich alunite corresponds to higher Pos1480 value. Pos1480 is a reliable vector to the heat source or porphyry that causes high sulfidation (HS) type mineralization, thereby it is helpful to detect high-grade epithermal Au ore bodies near the intrusion or the hidden porphyry orebody. The trace element contents of alunite obtained by LA-ICP-MS can more clearly track the ore body or porphyry. The Pb content in alunite decreases near the intrusion center, while Sr, La, La/Pb and Sr/Pb increase [3].

2.5. Exploration Indicator of REE-Bearing Minerals

The REE-related absorptions in the VNIR-SWIR bands for these LREE-enriched minerals can be largely attributed to the intraconfigurational 4f-4f electronic transitions of Pr³⁺, Nd³⁺, and Sm³⁺. Experimental studies about spectral features of economic REE-bearing minerals are conducted by Turner et al. (2014, 2016, 2018) [5–7]. The results show that REE fluorocarbonates (bastnäsite, synchysite, and parisite) are characterized by strong absorption peaks at 523, 580, 625, 676, 741, 792–798, 864, and 889 nm. REE phosphate minerals (monazite, xenotime, and britholite) can be defined by obvious absorption peaks at 745, 800, and 763–879 nm, but the spectral feature of monazite is relatively complex [5,6]. Tan et al. (2021, 2022) [8,42] conducted a systematic VNIR spectroscopy study on ion-exchangeable REEs. Several synthetic REE-adsorbed clay minerals and natural regolith samples were tested and compared. The results show that ion-exchangeable Nd³⁺, Dy³⁺, Ho³⁺, Er³⁺, and Tm³⁺ have diagnostic absorption peaks at 641, 652, 684, 730–870, and 805 nm. The Nd³⁺ related absorption peak at ~800 nm of regolith samples is suggested to characterize REE anomaly. The maxima of second derivative curves derived from the absorption peak at ~800 nm can be used to quantify variations of ion-exchangeable REEs in kaolinite, halloysite, illite, and montmorillonite [42] (Figure 5). The spectral parameter of

near 800 nm is effectively used to estimate the total REE concentrations in regolith profiles of the Renju regolith-hosted REE deposit, China [8].

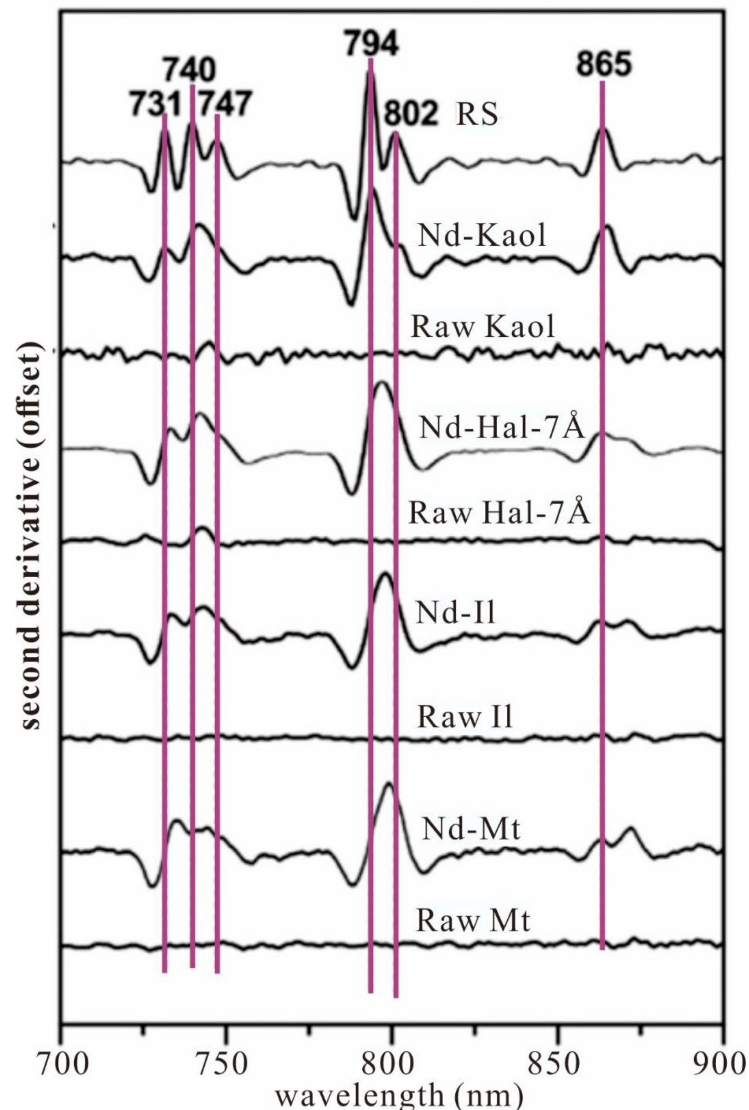


Figure 5. Secondary derivative reflectance spectra in the range of 700–900 nm (modified from [42]). RS—sample from the Renju REE deposit with a total REE concentration of 3340 ppm; Nd-Kaol—kaolinite with Nd content of 666.6 ppm; Raw Kaol—kaolinite with total REE concentration of below 50 ppm; Nd-Hal-7 Å—halloysite (7 Å) with Nd content of 1112.6 ppm; Raw Hal-7 Å—halloysite (7 Å) with total REE concentration of below 50 ppm; Nd-II—illite with Nd content of 1154.0 ppm; Raw II—illite with total REE concentration of below 50 ppm; Nd-Mt—montmorillonite with Nd content of 1087.3 ppm; Raw Mt—montmorillonite with total REE concentration of below 50 ppm.

2.6. Other MEIs

Mineral chemistry, with the aid of LA-ICP-MS technology, expands the range of prospecting forecasting, which is as effective as geophysics and geochemistry. More and more minerals can become research objects for MEIs.

The study conducted by Tian et al. (2019) [51] on secondary quartz of the Jiguanzui skarn Au-Cu deposit in Southeast Hubei revealed that the Al contents in metasomatic quartz and epithermal altered quartz are close, and they are both significantly higher than the quartz developed in an orogenic Au deposit and porphyry Au deposit. The Ti content of quartz in Jiguanzui is higher than in epithermal Au deposits but lower than in porphyry Au

deposits, and the variation of Ti content in quartz is positively correlated to the formation temperature. Al and Ti contents are potential exploration indicators [51].

Qiao et al. (2019) [52] and Li et al. (2020) [76] conducted detailed mineral chemistry and boron isotope studies on the tourmaline of the Hadamiao and Bilihe porphyry Au deposits in Yangzi Craton, Inner Mongolia. Six stages of tourmaline formation developed in the Hadamiao area consist of magmatic tourmaline, Au-bearing quartz-tourmaline-chalcopyrite vein, carbonate-tourmaline-quartz vein, and so on. The tourmaline with hydrothermal genesis has higher contents of Ba, Cu, and Y compared with magmatic tourmaline. The tourmaline in Au-bearing quartz-tourmaline-chalcopyrite vein has the lowest $\delta^{11}\text{B}$ (from -8.7‰ to -5.4‰), contrasting with the magmatic tourmaline with the highest $\delta^{11}\text{B}$ (from $+15.1\text{‰}$ to $+21.2\text{‰}$). The magmatic-hydrothermal fluid is proposed to supply light boron for hydrothermal tourmaline, and the widely distributed marine carbonate is proposed to supply heavy boron for magmatic tourmaline. The tourmaline of Bilihe presents similar features, and systematic contrasts in mineral chemistry suggest that V vs. Zn, ($\Sigma\text{REE} + \text{Y} + \text{Zr}$) vs. ($\text{Ni} + \text{V} + \text{Zn}$) and ($\text{Sn} + \text{Li}$) vs. ($\text{Ni} + \text{V} + \text{Zn}$) are potential elemental groups for identifying tourmaline in different environments [52,76].

Tang et al. (2019) [50] tried to distinguish the porphyry Cu (Mo) system and porphyry Mo (Cu) system of the Gangdise metallogenetic belt in Tibet with the aid of hydrothermal biotite chemistry. The hydrothermal biotite in the Cu (Mo) system has higher concentrations of Al_2O_3 , SiO_2 , MgO , K_2O , Na_2O , and F with lower contents of TiO_2 , FeO_t , MnO , and Cl, contrasted to the Mo (Cu) system. Based on the biotite chemical data, the formation temperature and the fluid oxygen fugacity in Cu (Mo) systems are also estimated to be higher and lower, respectively. It is implied that the two types of mineralization systems are formed by different magmatic-hydrothermal fluids [50]. Moshefi et al. (2018) [77] compared the geochemical characteristics of magmatic biotite and hydrothermal biotite in Sungun porphyry Cu-Mo deposits and found that the Cl content of biotite can be used as a vector for hydrothermal processes after the magmatic stage, and the F content is a potential indicator showing whether a porphyry system is fertile or barren [77].

2.7. Integrated MEIs from Multiple Alteration Minerals

The integrated MEIs are based on alteration mineral assemblage controlled by the physicochemical conditions of the mineralization fluid. MEI combinations can be more reliable predictors for prospecting and constraining the fluid features.

Spectroscopy big data show the spatial distributions of IC value, Pos2200 value, and Pos2250 value in the Fukeshan porphyry Cu-Mo deposit, Greater Xing'an Mountains: a high value of IC, Pos2200, and Pos2250 appeared where diorite and late magmatic veins developed. The highest Pos2200 and Pos2250 values are detected in the magmatic complex of the south Fukeshan area, which is regarded as the heat source. Further, the temperature is considered to be the critical factor controlling the MEIs in the Fukeshan area [76]. Fe-rich chlorite (Pos2250 > 2253 nm), kaolinite with high crystallinity (absorption peak value >2170 nm and absorption depth >0.18 of near 2165 nm), abnormal Pos2200 value (>2212 nm or <2202 nm) can be useful integrated MEIs in the Tongshankou skarn-porphyry Cu-Mo-W deposit [4].

With the aid of SWIR technology, You et al. (2021) [78] identified the mineralization-related alteration assemblage—pyrite—quartz—sericite—in the Aschele VMS Cu-Zn deposit, Xinjiang. The Pos2200 value decreases towards the direction of ore bodies and Pos2200 < 2205 nm corresponds to high-grade ore bodies. The Pos2250 value drops down from 2260 nm to 2250~2255 nm when approaching ore bodies [78]. Jones et al. (2005) [1] conducted a SWIR measure at the Myra Falls VMS deposit in Canada and found that the Pos2200 value near the ore body is relatively low and increases with regularity away from the ore body. This rule possibly occurs in every individual layer. Further analysis suggested the influence of rock composition on Pos2200 near the ore bodies is weak, but it is the most important factor for the Pos2200 of weakly altered rock. The Pos2250 value varies positively in correlation with Pos2200, given that Pos2200 < 2197 nm and Pos2250 < 2240 nm are the

potential vectors for prospecting [1]. Herrmann et al. (2001) [61] studied the Rosebery VMS Pb-Zn polymetallic deposit in Australia and found that the Pos2200 value declines from the distal end to the ore body, but the Pos2250 value seems random [61]. It is practicable to mark the bonanza with a relatively high Pos2200 value in the Hellyer VMS deposit in Australia and the Aroyo Rojo VMS deposit in Argentina [79,80].

3. Controlling Factors for the Behaviors of “The Pathfinder Elements”

The VNIR-SWIR and chemical indicators with regular spatial changes are defined by the geochemical behaviors of related elements (called the pathfinder elements), which are controlled by the physicochemical conditions of the mineralization environment. The existing element geochemistry knowledge can help with understanding the evolution of mineralization fluids, and with revealing the controlling factors of MEIs.

3.1. Temperature

In mineralization systems where temperature is the main variable, as the temperature increases; the lower the Al^{3+} content in sericite, the higher the IC value [2,66,81] (Figure 2a); and the higher the Fe content in chlorite [9,57,69,73] (Figure 2b), the higher the Na content in alunite [75] (Figure 2c).

The Ti content in chlorite has a clear positive correlation with temperature [9,40,71]. Titanium, which belongs to HFSEs, does not easily migrate in hydrothermal fluids, and the spatial variation of chlorite Ti content associated with propylitic zone has little correlation with fluid migration. Although there is no experimental evidence on the controlling factors for the geochemical behavior of Ti in chlorite, previous studies have proved that the Ti content of biotite is controlled by temperature. Chlorite has a similar lattice structure to biotite, thus it is reasonable that the Ti content of chlorite is also controlled by temperature [9].

Xiao et al. (2020) [40] studied the elemental migration of the alteration process from pyroxene, hornblende, and biotite to chlorite by using EPMA in three large porphyry Cu deposits of the Tuwu, Xinjiang, China, Atlas in the Philippines, the Atlas in the Philippines, and the Xiaokelehe in Daxing’anling, China. The TiO_2 content gradually decreased from biotite to chlorite, and titanite was also generated during the alteration process, suggesting that Ti^{4+} was supersaturated [40] (Figure 6). Further research suggests that the TiO_2 content in titanite may be controlled by the composition of the precursor minerals. The TiO_2 in chlorite has no obvious association with precursor minerals.

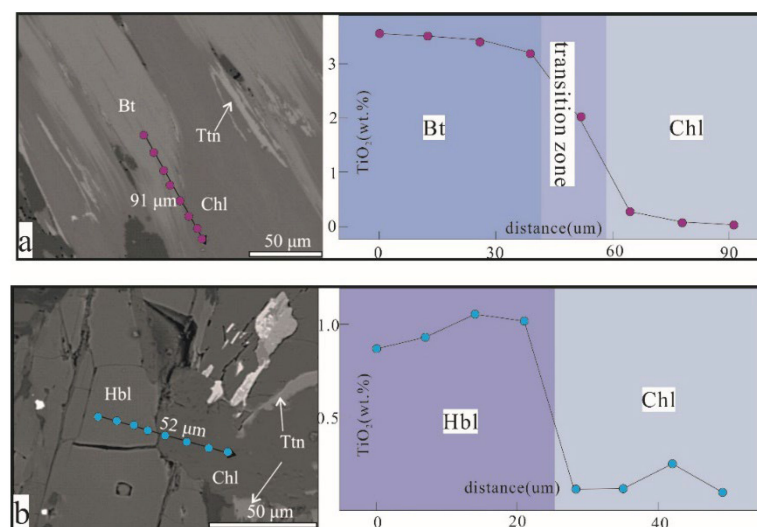
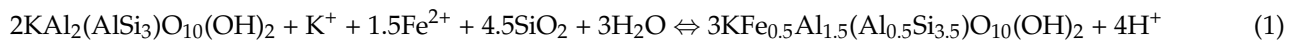


Figure 6. Concentration profiles of TiO_2 through biotite and hornblende to chlorite (modified from [40]). Bt—biotite; Chl—chlorite; Hbl—hornblende; Ttn—titanite.

3.2. The pH Value

In the epithermal environment with low lithostatic pressure, the most important controlling factors for the Al content of sericite are temperature and pH value [82]. Al content is higher in acidic environments due to the Tschermak substitution, which allows some of the Al^{3+} in the sericite lattice octahedron to be replaced by Fe^{2+} and Mg^{2+} . Taking muscovite and phengitic muscovite as an example, the following reaction occurs between them [26]:



That means the acidic environment will promote Al^{3+} entering the sericite lattice.

3.3. Other Controlling Factors

Wilkinson et al. (2015) [9] suggested that the spatial variation of chlorite Mn and Zn in porphyry systems may be related to the migration and spread of hydrothermal fluids. The content peak halo of chlorite Mn and Zn at about 800 m out of a porphyry-type ore body can be understood by the occurrence of the base metal (Pb, Zn, Mn, etc.) deposits at the periphery of the ore body of porphyry deposits [9]. Further explanation of the Mn and Zn behaviors of chlorite in the Batu Hijau deposit is that: the pyrite alteration halo, developed on the periphery of the potassic zone, hosted most of the Mn and Zn cations that entered the pyrite lattice, resulting in low Mn and Zn contents in chlorite and epidote. Outwards to the propylitic zone, the S^{2-} ions are almost exhausted, resulting in Mn and Zn cations entering the chlorite and epidote lattice, forming anomalies in mineral chemistry [9].

4. Research Directions

The development and research of MEIs are still in the initial stage and the previous work focused on the observation and statistics of the spatial variation of MEIs. The mineralization in different regions is distinct, which probably makes some MEIs invalid in the same type of deposits. Most MEI controlling factors have not yet been proven, which seriously restricts the promotion and application of MEIs.

Many MEI research cases have faced problems with the ambiguity of controlling factors. Feng et al. (2019) [83] regarded high Pos2250 value (>2245 nm) and low IC value (<0.8) as exploration indicators in the Xiaokelehe deposit due to their positive correlation and the directivity to the ore bodies. This is not easily explained by the single controlling factor of "temperature". Meanwhile, the chlorite chemistry and the other SWIR parameters seem spatially random [83]. Chen et al. (2019) [4] found the sericite SWIR parameters in the Tongshankou deposit show good correlation with a few ore bodies, but that the MEIs cannot be applied in the whole deposit. The regularity of chlorite Ti/Sr, Ti/Pb, and Mg/Sr values was not obvious [4]. Huang et al. (2018) [33] documented that the Pos2200 and Pos2250 values of the Honghai VMS Cu-Zn deposit in Xinjiang decreased when approaching the ore body, reflecting the sericite became relatively Al-rich and chlorite became relatively Mg-rich. The vicinity of ore bodies is characterized by a high temperature, making it unreasonable to simply use "temperature" to explain the spatial changes of the two indicators. Mg-rich seawater is considered to supply Mg^{2+} to chlorite, but further examination is lacking [33].

Alteration minerals are fingerprints left by hydrothermal mineralization processes, which are controlled by physicochemical conditions such as temperature, pressure, pH value, oxygen fugacity, sulfur fugacity, and the properties of the surrounding rock [17,18,84] (Figure 7). The study of ore deposits with an aim of examining the dividing alteration stage and fine alteration zone will help identify the possible spatiotemporal stage of fluid evolution, which is critical to the understanding of MEIs and their control factors. Based on the study of geological setting, lithology, mineralogy, and hydrothermal fluid, combined with alteration mapping, SWIR spectroscopy, and mineral chemistry, the MEIs of individual deposits can finally be confirmed. Before extracting the mineral chemical parameters, a small number of BSE, EPMA, and LA-ICP-MS tests are necessary to check whether the

test signal is straight and whether there are obvious zonal textures and inclusions in the mineral grains to ensure the mineral composition is homogeneous.

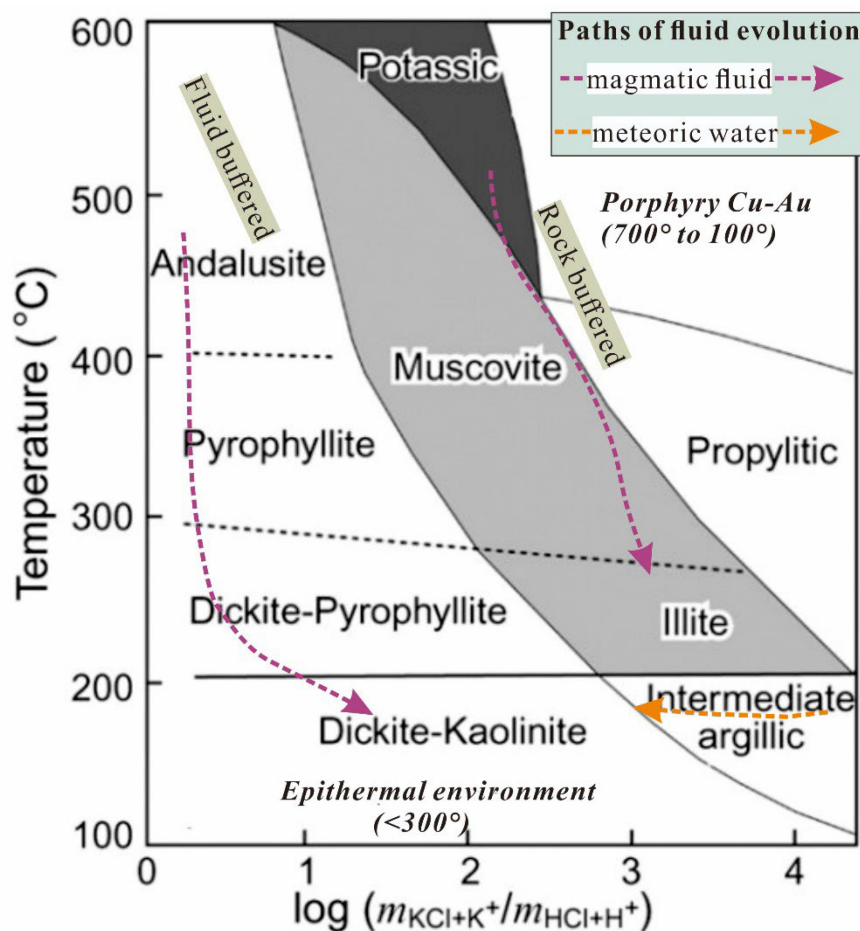


Figure 7. Phase diagram showing the alteration zones and their controlling factors in porphyry Cu-Au system and epithermal system (Modified from [84]). The phase boundaries are schematically constrained. The path of magmatic fluid on the left represents a fluid-dominant alteration sequence, whereas the one on the right illustrates rock-buffered alterations. A late influx of meteoric water into the porphyry environment forms the widespread rock-buffered intermediate argillic alteration.

Advances in effective spectral characterizing, with a focus on REE deposits, inspired us to develop more direct exploration indicators for some of the critical minerals that play a significant role in our economy, and in renewable energy development. Further experiments on critical element-bearing minerals through the use of infrared spectroscopy are advised. A significant knowledge gap exists between the fields of hyperspectral reflectance spectroscopy and critical mineralogy.

More spectral and chemical data accumulation for relevant minerals, more cases, and more multi-method joint research activities are needed to reveal the controlling factors of MEIs and the properties of mineralization fluid, and to improve the theoretical foundation.

Author Contributions: Investigation, Y.Z.; resources, Y.Z., W.G. and G.X.; data curation, T.W. and F.F.; writing—original draft preparation, Y.Z. and S.C.; writing—review and editing, J.S.; visualization, F.X.; supervision, Y.Z. All authors have read and agreed to the published version of the manuscript.

Funding: This research was funded by China Geological Survey (project numbers DD20221688 and DD20221803) and The National High Technology Research and Development Program of China (Grant No. 2016YFC0600210).

Data Availability Statement: Not applicable.

Acknowledgments: We give special thanks to Huayong Chen and Bing Xiao for their valuable and constructive comments that greatly improved the quality of the manuscript. Two anonymous reviewers and are greatly thanked for their valuable and constructive comments.

Conflicts of Interest: We declare that we have no financial and personal relationships with other people or organizations that can inappropriately influence our work, there is no professional or other personal interest of any nature or kind in any product, service and/or company that could be construed as influencing the position presented in, or the review of, the manuscript entitled.

References

1. Jones, S.; Herrmann, W.; Gemmell, J.B. Short wavelength infrared spectral characteristics of the HW Horizon: Implications for exploration in the Myra Falls volcanic-hosted massive sulfide camp, Vancouver Island, British Columbia, Canada. *Econ. Geol.* **2005**, *2*, 273–294. [[CrossRef](#)]
2. Yang, Z.M.; Hou, Z.Q.; Yang, Z.S.; Qu, H.C.; Li, Z.Q.; Liu, Y.F. Application of short wavelength infrared (SWIR) technique in exploration of poorly eroded porphyry Cu district: A case study of Niancun ore district, Tibet. *Min. Depos.* **2012**, *31*, 699–717, (In Chinese with English Abstract).
3. Chang, Z.S.; Hedenquist, J.W.; White, N.C.; Cooke, D.R.; Roach, M.; Deyell, C.L.; Garcia, J.; Gemmell, J.B.; McKnight, S.; Cuison, A.L. Exploration tools for linked porphyry and epithermal deposits: Example from the Mankayan Intrusion-centered Cu-Au district, Luzon, Philippines. *Econ. Geol.* **2011**, *106*, 1365–1398. [[CrossRef](#)]
4. Chen, H.Y.; Zhang, S.T.; Chu, G.B.; Zhang, Y.; Cheng, J.M.; Tian, J.; Han, J.S. The short-wave infrared (SWIR) spectral characteristics of alteration minerals and applications for ore exploration in the typical skarn-porphyry deposits, Edong ore district, eastern China. *Acta Petrol. Sin.* **2019**, *35*, 3629–3643, (In Chinese with English Abstract).
5. Turner, D.J.; Rivard, B.; Groat, L.A. Visible and short-wave infrared reflectance spectroscopy of REE fluorocarbonates. *Am. Mineral.* **2014**, *99*, 1335–1346. [[CrossRef](#)]
6. Turner, D.J.; Rivard, B.; Groat, L.A. Visible and short-wave infrared reflectance spectroscopy of REE phosphate minerals. *Am. Mineral.* **2016**, *101*, 2264–2278. [[CrossRef](#)]
7. Turner, D.J.; Rivard, B.; Groat, L.A. Visible and short-wave infrared reflectance spectroscopy of selected REE-bearing silicate minerals. *Am. Mineral.* **2018**, *103*, 927–943. [[CrossRef](#)]
8. Tan, W.; Qin, X.; Liu, J.; Zhou, M.F.; He, H.; Yan, W.C.; Huang, J.; Zhu, J.; Yao, Y.; Cudahy, T. Feasibility of visible short-wave infrared reflectance spectroscopy to characterize regolith-hosted rare earth element mineralization. *Econ. Geol.* **2022**, *117*, 495–508. [[CrossRef](#)]
9. Wilkinson, J.J.; Chang, Z.; Cooke, D.R.; Baker, M.J.; Wilkinson, C.C.; Inglis, S.; Chen, H.; Bruce Gemmell, J. The chlorite proximitor: A new tool for detecting porphyry ore deposits. *J. Geochem. Explor.* **2015**, *152*, 10–26. [[CrossRef](#)]
10. Maryono, A.; Harrison, R.L.; Rompo, I.; Priowasono, E.; Norris, M. Successful techniques in exploring the lithocaps environment of Sunda magmatic arc, Indonesia. In Proceedings of the 8th MGEI Annual Convention, Bandung, Indonesia, 21 June 2016; pp. 7–13.
11. Izawa, E.; Hayashi, T. Potential for Porphyry Copper Mineralization Below the Kasuga Lithocap, Nansatsu District, Japan: Potential for porphyry Cu below Kasuga lithocap. *Resour. Geol.* **2018**, *68*, 181–194. [[CrossRef](#)]
12. Cooke, D.R.; Agnew, P.; Hollings, P.; Baker, M.; Chang, Z.; Wilkinson, J.J.; Ahmed, A.; White, N.C.; Zhang, L.; Thompson, J.; et al. Recent advances in the application of mineral chemistry to exploration for porphyry copper–gold–molybdenum deposits: Detecting the geochemical fingerprints and footprints of hypogene mineralization and alteration. *Geochem. Explor. Environ. Anal.* **2020**, *20*, 176–188. [[CrossRef](#)]
13. Hedenquist, J.W.; Taran, Y.A. Modeling the Formation of Advanced Argillic Lithocaps: Volcanic Vapor Condensation Above Porphyry Intrusions. *Econ. Geol.* **2013**, *108*, 1523–1540. [[CrossRef](#)]
14. Lecumberri-Sanchez, P.; Newton, M.C.; Westman, E.C.; Kamilli, R.J.; Canby, V.M.; Bodnar, R.J. Temporal and spatial distribution of alteration, mineralization and fluid inclusions in the transitional high-sulfidation epithermal–porphyry copper system at Red Mountain, Arizona. *J. Geochem. Explor.* **2013**, *125*, 80–93. [[CrossRef](#)]
15. Cooke, D.R.; White, N.C.; Zhang, L.J.; Chang, Z.S.; Chen, H.Y. Lithocaps: Characteristics, origins and significance for porphyry and epithermal exploration. In Proceedings of the 14th SGA Biennial Meeting, Quebec City, QC, Canada, 20–23 August 2017; Australian Research Council: Lancaster, Australia, 2017; Volume 1, pp. 291–294.
16. Chen, H.Y. Meditations on the future development of ore deposit science in China. *Earth Sci. Front.* **2020**, *27*, 99–105, (In Chinese with English Abstract).
17. Holliday, R.J.; Cooke, D. Advances in geological models and exploration methods for copper ± gold porphyry deposits. *Ore Depos. Expl. Techn.* **2007**, *7*, 791–809.
18. Sillitoe, R.H. Porphyry copper systems: An invited paper. *Econ. Geol.* **2010**, *105*, 3–41. [[CrossRef](#)]
19. Sillitoe, R.H. Geological criteria for porphyry copper exploration. *Acta Geol. Sin. Engl. Ed.* **2014**, *88*, 597–598. [[CrossRef](#)]
20. Zadeh, M.H.; Tangestani, M.H.; Roldan, F.V.; Yusta, I. Spectral characteristics of minerals in alteration zones associated with porphyry copper deposits in the middle part of Kerman copper belt, SE Iran. *Ore Geol. Rev.* **2014**, *62*, 191–198. [[CrossRef](#)]
21. Zhang, T.J.; Chen, Y.; Zhang, C.J. Discussion on Changdagou porphyry copper deposits mineralization model in Dege, Sichuan Province. *Acta Geol. Sin. Engl. Ed.* **2014**, *88*, 651–652.

22. Li, Y.; Su, C.; Wang, X.; Huang, Z.; Zhang, X. Extraction of alteration information and establishment of prospecting model for porphyry copper-gold deposits in Luzon. *Rem. Sens. Techn. Appl.* **2017**, *32*, 1151–1160.
23. Testa, F.J.; Villanueva, C.; Cooke, D.R.; Zhang, L.J. Lithological and hydrothermal alteration mapping of epithermal, porphyry and tourmaline breccia districts in the Argentine Andes using ASTER imagery. *Rem. Sens.* **2018**, *10*, 203. [[CrossRef](#)]
24. Yazdi, Z.; Rad, A.J.; Aghazadeh, M.; Afzal, P. Alteration Mapping for Porphyry Copper Exploration Using ASTER and QuickBird Multispectral Images, Sonajeel Prospect, NW Iran. *J. Indian Soc. Remote* **2018**, *46*, 1581–1593. [[CrossRef](#)]
25. Mao, J.W.; Zhou, T.F.; Xie, G.Q.; Yuan, F.; Duan, C. Metallogeny in Middle-Lower Yangtze River Ore Belt: Advances and problems remained. *Min. Depos.* **2020**, *39*, 547–558, (In Chinese with English Abstract).
26. Halley, S.; Dilles, J.; Tosdal, R. Footprints: Hydrothermal alteration and geochemical dispersion around porphyry copper deposits. *SEG Newsl.* **2015**, *100*, 11–17. [[CrossRef](#)]
27. Xiu, L.C.; Zheng, Z.Z.; Yin, L.; Chen, C.X.; Yu, Z.K.; Huang, B.; Zhang, Q.N.; Xiu, X.X.; Gao, Y. Research on assessment methods of spectrum data quality of core scan. *Spectr. Spectr. Anal.* **2015**, *35*, 2352–2356, (In Chinese with English Abstract).
28. Cooke, D.R.; Hollings, P.; Wilkinson, J.J.; Tosdal, R.M. Geochemistry of Porphyry Deposits. In *Treatise on Geochemistry*; Elsevier: Amsterdam, The Netherlands, 2014; pp. 357–381.
29. Lu, Y.; Zhou, Y.; Zhang, H.L.; Yang, K.; Chen, S.Z.; Xi, W.W.; Xiu, L.C.; Xing, G.F. Hydrothermal alteration and its significance for exploration at the Dongji gold-silver deposit in Zhenghe, Fujian province. *Geol. Expl.* **2017**, *53*, 1039–1050, (In Chinese with English Abstract).
30. Wang, R.; Cudahy, T.; Laukamp, C.; Walshe, J.L.; Bath, A.; Mei, Y.; Young, C.; Roache, T.J.; Jenkins, A.; Roberts, M.; et al. White Mica as a Hyperspectral Tool in Exploration for the Sunrise Dam and Kanowna Belle Gold Deposits, Western Australia. *Econ. Geol.* **2017**, *112*, 1153–1176.
31. Guo, N.; Huang, Y.L.; Zheng, L.; Tang, N.; Fu, Y.; Wang, C. Alteration zoning and prospecting model of epithermal deposit revealed by shortwave infrared technique: A case study of Tiegelongnan and Sinongduo deposits. *Acta Geosci. Sin.* **2017**, *38*, 767–778, (In Chinese with English Abstract).
32. Guo, N.; Shi, W.X.; Huang, Y.R.; Zheng, L.; Tang, N.; Wang, C.; Fu, Y. Alteration mapping and prospecting model construction in the Tiegelongnan ore deposit of the Duolong ore concentration area, northern Tibet, based on shortwave infrared technique. *Geol. Bull. China* **2018**, *37*, 446–457, (In Chinese with English Abstract).
33. Huang, J.; Chen, H.; Han, J.; Deng, X.; Lu, W.; Zhu, R. Alteration zonation and short wavelength infrared (SWIR) characteristics of the Honghai VMS Cu-Zn deposit, Eastern Tianshan, NW China. *Ore Geol. Rev.* **2018**, *100*, 263–279.
34. Tian, F.; Leng, C.B.; Zhang, X.C.; Tian, Z.D.; Zhang, W.; Guo, J.H. Application of short-wave infrared spectroscopy in the Gangjiang porphyry Cu-Mo deposit in the Nimu ore field, Tibet. *Earth Sci.* **2019**, *44*, 2143–2154, (In Chinese with English Abstract).
35. Zhou, Y.; Xiu, L.C.; Yang, K.; Zhang, H.L.; Chen, S.Z.; Fan, F.P.; Xiao, F. Development and application of infrared spectrum mineral mapping technique. *East China Geol.* **2019**, *40*, 289–298, (In Chinese with English Abstract).
36. Zhou, Y.; Li, L.M.; Yang, K.; Xing, G.F.; Xiao, W.J.; Zhang, H.L.; Xiu, L.C.; Yao, Z.Y.; Xie, Z.J. Hydrothermal alteration characteristics of the Chating Cu-Au deposit in Xuancheng City, Anhui Province, China: Significance of sericite alteration for Cu-Au exploration. *Ore Geol. Rev.* **2020**, *127*, 103844. [[CrossRef](#)]
37. Cao, Y.; Li, S.R.; Shen, J.F.; Yao, M.J.; Li, Q.K.; Mao, F.L. Application of portable infrared mineral analyzer (PIMA) in the Qianhe gold mine, Henan province. *Geol. Prospect.* **2008**, *44*, 82–86, (In Chinese with English Abstract).
38. Huang, Y.; Guo, N.; Zheng, L.; Yang, Z.; Fu, Y. 3D geological alteration mapping based on remote sensing and shortwave infrared technology: A case study of the Sinongduo low-sulfidation epithermal deposit. *Acta Geosci. Sin.* **2017**, *38*, 779–789.
39. Xiao, B.; Chen, H.; Wang, Y.; Han, J.; Xu, C.; Yang, J. Chlorite and epidote chemistry of the Yandong Cu deposit, NW China: Metallogenic and exploration implications for Paleozoic porphyry Cu systems in the Eastern Tianshan. *Ore Geol. Rev.* **2018**, *100*, 168–182. [[CrossRef](#)]
40. Xiao, B.; Chen, H. Elemental behavior during chlorite alteration: New insights from a combined EMPA and LA-ICPMS study in porphyry Cu systems. *Chem. Geol.* **2020**, *543*, 119604. [[CrossRef](#)]
41. Tang, N.; Tang, J.X.; Guo, N.; Lin, B.; Wang, Q.; Yang, C. Application of short-wave infrared spectrometer in the study of alteration zoning of ore deposits: A case study of Tiegelongnan porphyry-epithermal hydrothermal deposit in Tibet. *Acta Miner. Sin.* **2015**, *35*, 925–926. (In Chinese)
42. Tan, W.; Qin, X.; Liu, J.; Michalski, J.; He, H.; Yao, Y.; Yang, M.; Huang, J.; Lin, X.; Zhang, C.; et al. Visible/near infrared reflectance (VNIR) spectral features of ion-exchangeable rare earth elements hosted by clay minerals: Potential use for exploration of regolith-hosted REE deposits. *Appl. Clay Sci.* **2021**, *215*, 106320. [[CrossRef](#)]
43. He, G.H.; Zhou, T.F.; Fan, Y.; Wang, S.W.; Xiao, Q.L. Geochemical characteristics and exploration implications of chlorite in Shaxi porphyry copper gold deposit, Lujiang. *Min. Depos.* **2018**, *37*, 1247–1259, (In Chinese with English Abstract).
44. Zhang, S.; Xiao, B.; Long, X.; Chu, G.; Cheng, J.; Zhang, Y.; Tian, J.; Xu, G. Chlorite as an exploration indicator for concealed skarn mineralization: Perspective from the Tonglushan Cu-Au-Fe skarn deposit, Eastern China. *Ore Geol. Rev.* **2020**, *126*, 103778. [[CrossRef](#)]
45. Wilkinson, J.J.; Baker, M.J.; Cooke, D.R.; Wilkinson, C.C. Exploration Targeting in Porphyry Cu Systems Using Propylitic Mineral Chemistry: A Case Study of the El Teniente Deposit, Chile. *Econ. Geol.* **2020**, *115*, 771–791. [[CrossRef](#)]
46. Baker, M.J.; Wilkinson, J.J.; Wilkinson, C.C.; Cooke, D.R.; Ireland, T. Epidote Trace Element Chemistry as an Exploration Tool in the Collahuasi District, Northern Chile. *Econ. Geol.* **2020**, *115*, 749–770. [[CrossRef](#)]

47. Xiao, B.; Chu, G.; Feng, Y. Short-wave infrared (SWIR) spectral and geochemical characteristics of hydrothermal alteration minerals in the Laowangou Au deposit: Implications for ore genesis and vectoring. *Ore Geol. Rev.* **2021**, *139*, 104463. [[CrossRef](#)]
48. Alva-Jimenez, T.; Tosdal, R.M.; Dilles, J.H.; Dipple, G.; Kent, A.J.R.; Halley, S. Chemical Variations in Hydrothermal White Mica Across the Highland Valley Porphyry Cu-Mo District, British Columbia, Canada. *Econ. Geol.* **2020**, *115*, 903–926. [[CrossRef](#)]
49. Ahmed, A.D.; Fisher, L.; Pearce, M.; Escolme, A.; Cooke, D.R.; Howard, D.; Belousov, I. A Microscale Analysis of Hydrothermal Epidote: Implications for the Use of Laser Ablation-Inductively Coupled Plasma-Mass Spectrometry Mineral Chemistry in Complex Alteration Environments. *Econ. Geol.* **2020**, *115*, 793–811. [[CrossRef](#)]
50. Tang, P.; Tang, J.; Lin, B.; Wang, L.; Zheng, W.; Leng, Q.; Gao, X.; Zhang, Z.; Tang, X. Mineral chemistry of magmatic and hydrothermal biotites from the Bangpu porphyry Mo (Cu) deposit, Tibet. *Ore Geol. Rev.* **2019**, *115*, 103122. [[CrossRef](#)]
51. Tian, F.; Leng, C.B.; Zhang, X.C.; Tian, Z.D.; Zhang, W.; Guo, J.H. Application of short wavelength infrared technique in exploration of mineral deposit: A review. *Bull. Mineral. Petrol. Geochem.* **2019**, *38*, 1–9, (In Chinese with English Abstract).
52. Qiao, X.; Li, W.; Zhang, L.; White, N.C.; Zhang, F.; Yao, Z. Chemical and boron isotope compositions of tourmaline in the Hadamiao porphyry gold deposit, Inner Mongolia, China. *Chem. Geol.* **2019**, *519*, 39–55. [[CrossRef](#)]
53. Li, W.; Qiao, X.; Zhang, F.; Zhang, L. Tourmaline as a potential mineral for exploring porphyry deposits: A case study of the Bilihe gold deposit in Inner Mongolia, China. *Miner. Depos.* **2022**, *57*, 61–82. [[CrossRef](#)]
54. Kübler, B. La cristallinité de l'illite et les zones tout à fait supérieures du métamorphisme. La Cristallinité de L'illite et les Zones Tout À Fait Supérieures du Métamorphisme. Etages tectoniques, In Proceedings of Colloque de Neuchâtel, Neuchâtel, Switzerland, 18–21 April 1966; pp. 105–121.
55. McLeod, R.L.; Gabbell, A.R.; Green, A.A.; Gardavsky, V. Chlorite infrared spectral data as proximity indicators of volcanogenic massive sulfide mineralization. In Proceedings of the Pacific Rim Congress, Auckland, New Zealand, 26–29 August 1987; pp. 321–324.
56. Scott, K.M.; Yang, K. Spectral reflectance studies of white micas. In *CSIRO Exploration and Mining Report 439R*; Commonwealth Scientific and Industrial Research Organisation (CSIRO): Sydney, Australia, 1997.
57. Yang, K.; Lian, C.; Huntington, J.F.; Peng, Q.; Wang, Q. Infrared spectral reflectance characterization of the hydrothermal alteration at the Tuwu Cu-Au deposit, Xinjiang, China. *Miner. Depos.* **2005**, *40*, 324–336. [[CrossRef](#)]
58. Thompson, A.J.B.; Hauff, P.; Robitaille, A.J. Alteration mapping in exploration: Application of short-wave infrared (SWIR) spectroscopy. *SEG Newsl.* **1999**, *39*, 16–27. [[CrossRef](#)]
59. Duke, E.F. Near infrared spectra of muscovite, Tschermak substitution, and metamorphic reaction progress: Implications for remote sensing. *Geology* **1994**, *22*, 621. [[CrossRef](#)]
60. Chaffee, M.A. A geochemical study of the Kalamazoo porphyry copper deposit, Pinal County, Arizona. In *Advances in Geology of the Porphyry Copper Deposits*; Titley, S.R., Ed.; The University of Arizona Press: Tucson, AZ, USA, 1982; pp. 211–225.
61. Herrmann, W.; Blake, M.; Doyle, M.; Huston, D.; Kamprad, J.; Merry, N.; Pontual, S. Short wavelength infrared (SWIR) spectral analysis of hydrothermal alteration zones associated with base metal sulfide deposits at Rosebery and Western Tharsis, Tasmania, and Highway-Reward, Queensland. *Econ. Geol.* **2001**, *96*, 939–955. [[CrossRef](#)]
62. Sun, Y.Y.; Secombe, P.K.; Yang, K. Application of short-wave infrared spectroscopy to define alteration zones associated with the Elura zinc-lead-silver deposit, NSW, Australia. *J. Geochem. Explor.* **2001**, *73*, 11–26. [[CrossRef](#)]
63. Thompson, A.J.B.; Scott, K.; Huntington, J.; Yang, K. Mapping mineralogy with reflectance spectroscopy: Examples from volcanogenic massive sulfide deposits. *Rev. Econ. Geol.* **2009**, *16*, 25–40.
64. Howard, N. Geochemistry and hydrothermal alteration at the Mount Rawdon gold deposit. In *New England Orogen Geology, Tectonics, Economics*; Australian Institute of Geoscientists Seminar Series; Australian Institute of Geoscientists: Brisbane, Australia, 2015; pp. 1–8.
65. Laakso, K.; Peter, J.M.; Rivard, B.; White, H.P. Short-wave infrared spectral and geochemical characteristics of hydrothermal alteration at the Archean Izok Lake Zn-Cu-Pb-Ag volcanogenic massive sulfide deposit, Nunavut, Canada: Application in exploration target vectoring. *Econ. Geol.* **2016**, *111*, 1223–1239. [[CrossRef](#)]
66. Xu, C.; Chen, H.Y.; Noel, W.; Qi, J.P.; Zhang, L.J.; Zhang, S.; Duan, G. Alteration and mineralization of Xinan Cu-Mo ore deposit in Zijinshan orefield, Fujian Province, and application of short wavelength infra-red technology (SWIR) to exploration. *Min. Depos.* **2017**, *36*, 1013–1038, (In Chinese with English Abstract).
67. Yang, K.; Huntington, J.F.; Scott, K.M. Spectral characterization of the hydrothermal alteration at Hishikari, Japan. In Proceedings of the Water-Rock Interaction, Taupo, New Zealand, 30 March–3 April 1998; Balkema: Rotterdam, The Netherlands; Brookfield, VT, USA, 1998; pp. 587–590.
68. Simpson, M.P. Reflectance spectrometry (SWIR) of alteration minerals surrounding the Favona epithermal vein, Waihi vein system, Hauraki Goldfield. In Proceedings of the Australasian Institute of Mining and Metallurgy New Zealand Branch Conference, Dunedin, New Zealand, 31 August 2015; pp. 409–418.
69. Han, J.S.; Chu, G.B.; Chen, H.Y.; Hollings, P.; Sun, S.Q.; Chen, M. Hydrothermal alteration and short wavelength infrared (SWIR) characteristics of the Tongshankou porphyry-skarn Cu-Mo deposit, Yangtze craton, Eastern China. *Ore Geol. Rev.* **2018**, *101*, 143–164. [[CrossRef](#)]
70. Pacey, A.; Wilkinson, J.J.; Cooke, D.R. Chlorite and Epidote Mineral Chemistry in Porphyry Ore Systems: A Case Study of the Northparkes District, New South Wales, Australia. *Econ. Geol.* **2020**, *115*, 701–727. [[CrossRef](#)]

71. Wilkinson, J.J.; Pacey, A.; Hart-Madigan, L.A.; Longridge, J.; Cooke, D.R.; Baker, M.J.; Boyce, A.J.; Wilkinson, C.C. A new paradigm for the origin of propylitic alteration in porphyry ore systems. *Appl. Earth Sci.* **2019**, *128*, 64–65. [[CrossRef](#)]
72. Cooke, D.R.; Wilkinson, J.J.; Baker, M.; Agnew, P.; Phillips, J.; Chang, Z.; Chen, H.; Wilkinson, C.C.; Inglis, S.; Hollings, P.; et al. Using Mineral Chemistry to Aid Exploration: A Case Study from the Resolution Porphyry Cu-Mo Deposit, Arizona. *Econ. Geol.* **2020**, *115*, 813–840. [[CrossRef](#)]
73. Zhang, S.T.; Chen, H.Y.; Zhang, X.B.; Zhang, W.F.; Xu, C. Application of short wavelength infrared (SWIR) technique in exploration of skarn deposit: A case study of the Tonglvshan Cu-Fe-Au deposit, Edongnan ore district, Hubei Province. *Min. Depos.* **2017**, *36*, 1263–1288, (In Chinese with English Abstract).
74. Sillitoe, R.H. Exploration of porphyry copper lithocaps. *Proc. Pac. Rim Congr.* **1995**, *9*, 527–532.
75. Stoffregen, R.E.; Cygan, G.L. An experimental study of Na-K exchange between alunite and aqueous sulfate solutions. *Am. Mineral.* **1990**, *75*, 209–220.
76. Li, R.C.; Chen, H.Y.; Li, G.H.; Feng, Y.Z.; Xiao, B.; Han, J.S.; Deng, C.Z.; Shi, H.L. Geological characteristics and application of short wavelength infra-red technology (SWIR) in the Fukeshan porphyry copper deposit in the Great Xing'an Range area. *Earth Sci.* **2020**, *45*, 1517–1530, (In Chinese with English Abstract).
77. Moshefi, P.; Hosseinzadeh, M.R.; Moayyed, M.; Lentz, D.R. Comparative study of mineral chemistry of four biotite types as geochemical indicators of mineralized and barren intrusions in the Sungun porphyry Cu-Mo deposit, northwestern Iran. *Ore Geol. Rev.* **2018**, *97*, 1–20. [[CrossRef](#)]
78. You, F.H.; Jiang, J.J.; Zhang, J.Z.; Lai, X.D. Application of short-wave infrared technique in exploration of Ashele Cu-Zn deposit in Xinjiang. *Acta Petrol. Mineral.* **2021**, *40*, 1010–1022, (In Chinese with English Abstract).
79. Yang, K.; Huntington, J.F.; Gemmell, J.B.; Scott, K.M. Variation in composition and abundance of white mica in the hydrothermal alteration system at Hellyer, Tasmania, as revealed by infrared reflectance spectroscopy. *J. Geochem. Explor.* **2011**, *108*, 143–156.
80. Biel, C.; Subías, I.; Acevedo, R.D.; Yusta, I.; Velasco, F. Mineralogical, IR-spectral and geochemical monitoring of hydrothermal alteration in a deformed and metamorphosed Jurassic VMS deposit at Arroyo Rojo, Tierra del Fuego, Argentina. *J. S. Am. Earth Sci.* **2012**, *35*, 62–73.
81. Chang, Z.S.; Yang, Z.M. Evolution of inter-instrument variation among short wavelength infrared (SWIR) devices. *Econ. Geol.* **2012**, *107*, 1479–1488. [[CrossRef](#)]
82. Yang, K.; Huntington, J.F.; Boardman, J.W.; Mason, P. Mapping hydrothermal alteration in the Comstock mining district, Nevada, using simulated satellite-borne hyperspectral data. *J. Geol. Soc. Aust.* **2001**, *46*, 915–922. [[CrossRef](#)]
83. Feng, Y.; Xiao, B.; Li, R.; Deng, C.; Han, J.; Wu, C.; Li, G.; Shi, H.; Lai, C. Alteration mapping with short wavelength infrared (SWIR) spectroscopy on Xiaokelehe porphyry Cu-Mo deposit in the Great Xing'an Range, NE China: Metallogenic and exploration implications. *Ore Geol. Rev.* **2019**, *112*, 103062. [[CrossRef](#)]
84. Seedorff, E.; Dilles, J.H.; Proffett, J.M.; Einaudi, M.T.; Zurcher, L.; Stavast, W.J.A.; Barton, M.D.; Johnson, D.A. Porphyry-related deposits: Characteristics and origin of hypogene features. In *Economic Geology 100th Anniversary Volume*; Society of Economic Geologists: Littleton, CO, USA, 2005; pp. 251–298.